Analytica Chimica Acta 1338 (2025) 343601

Contents lists available at ScienceDirect

Analytica Chimica Acta

journal homepage: www.elsevier.com/locate/aca

CRISPR-associated Plasmonic Colorimeter Method (Ca-PCM): A real-time RGB detection system for gold nanoparticles-based nucleic acid biosensors

Hernán Alarcón-Iniesta [a,1], Guillermo de Arana [a,1], María López-Valls [a], Demian Pardo [a], Carmen Escalona-Noguero [a], Ciro Rodríguez [a], Milagros Castellanos [a], Sara Cobelo [a], Isidoro Martínez-Ramírez [a,b], Julio Camarero [a,c], Sergio de las Heras [a], Javier de Vicente [a], Andrés Valera [a], Warren Smith [a], Ramón Bernardo-Gavito [a], Rafael Cantón [d,e], Juan Carlos Galán [d,f], Daniel Granados [a], Rodolfo Miranda [a,c], Héctor Guerrero [a,**], Begoña Sot [g,h,a,*]

[a] Fundación IMDEA Nanociencia, Madrid, Spain
[b] Departamento de Física Aplicada a las Ingenierías Aeronáutica y Naval, E.T.S.I. Aeronáutica y del Espacio, Universidad Politécnica de Madrid (UPM), 28040, Madrid, Spain
[c] Departamento de Física de la Materia Condensada, Universidad Autónoma de Madrid, Madrid, Spain
[d] Servicio de Microbiología, Hospital Universitario Ramón y Cajal and Instituto Ramón y Cajal de Investigación Sanitaria (IRYCIS), 28034, Madrid, Spain
[e] Centro de Investigación Biomédica en Red (CIBER) en Enfermedades Infecciosas, Instituto de Salud Carlos III. Madrid, Spain (CIBERINFEC), Spain
[f] Centro de Investigación Biomédica en Red (CIBER) en Epidemiología y Salud Pública, Instituto de Salud Carlos III. Madrid, Spain.(CIBERESP), Spain
[g] Division of Hematopoietic Innovative Therapies, Innovative Therapies Unit. Centro de Investigaciones Energéticas, Medioambientales y Tecnológicas (CIEMAT), 28040, Madrid, Spain
[h] Advanced Therapies Unit, Instituto de Investigación Sanitaria Fundación Jiménez Díaz (IIS-FJD, UAM), 28040, Madrid, Spain

HIGHLIGHTS

- Ca-PCM enables RNA detection using AuNP aggregation and real-time RGB measurements.
- Analysis of temporal spectral patterns allows dose-dependent target detection.
- Ca-PCM can be coupled with one-pot/two-step isothermal amplification.
- One-pot/two-step Ca-PCM is compatible for the evaluation of clinical samples.
- A new method for exploiting plasmonic-based biosensors is demonstrated.

GRAPHICAL ABSTRACT

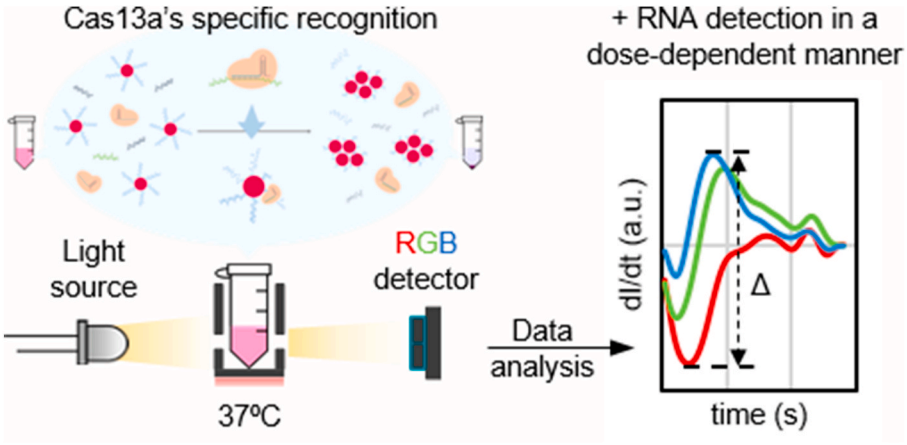

* Corresponding author. Division of Hematopoietic Innovative Therapies, Innovative Therapies Unit. Centro de Investigaciones Energéticas, Medioambientales y Tecnológicas (CIEMAT), 28040, Madrid, Spain.
** Corresponding author.
E-mail addresses: hector.guerrero@ciencia.gob.es (H. Guerrero), mbegona.sot@ciemat.es (B. Sot).
[1] These authors contributed equally to this work.

https://doi.org/10.1016/j.aca.2024.343601
Received 30 April 2024; Received in revised form 3 December 2024; Accepted 29 December 2024
Available online 30 December 2024

ARTICLE INFO

Handling Editor: Prof Nicola Cioffi

Keywords:
Real-time RGB
Biosensor
CRISPR/Cas
Gold nanoparticles
RNA detection

ABSTRACT

Background: The detection of genetic sequences represents the gold standard procedure for species discrimination, genetic characterisation of tumours, and identification of pathogens. The development of new molecular detection methods, accessible and cost effective, is of great relevance. Biosensors based on plasmonic nanoparticles, such as gold nanoparticles (AuNPs), provide a powerful and versatile platform for highly sensitive, economic, user-friendly and label-free sensing. However, the readout techniques typically employed with such sensors lack temporal and kinetic information, which hampers the ability to perform quantitative detection.
Results: In this study, a novel methodology designated the 'CRISPR-associated Plasmonic Colorimeter Method' (Ca-PCM), has been developed. This method combines RNA target recognition by CRISPR LwaCas13a, AuNPs' aggregation, and real-time colorimetric Red-Green-Blue (RGB) analysis. The system registers the AuNP's plasmonic signatures in real-time using a RGB colour sensor with 3-channel silicon photodiodes having blue, green and red sensitivities. The acquired signals are automatically analysed by an algorithm designed to distinguish between positive and negative samples and to correlate the temporal spectral patterns of aggregation with dose-dependent molecular detection of the RNA target. In addition, the combination of Ca-PCM with a previous isothermal amplification allows the target efficient detection in real clinical applications.
Significance: We have shown that the combination of RGB analysis and continuous temporal measurements is a novel and promising method to characterise the behaviour of gold nanoparticle-based biosensors and to achieve dose-dependent target detection. In addition, the simplicity and cost-effectiveness of this new approach expand the possibilities of other plasmonic-based biosensors and their applicability in low-resources clinical environments.

1. Introduction

Nucleic acid detection is a fundamental tool for diagnosing pathogenic or genetic diseases. Quantitative polymerase chain reaction (qPCR) is the most commonly used technique for this purpose. However, it requires the utilisation of specialised instrumentation and the input of trained personnel, and therefore it must be performed in fully equipped molecular diagnosis laboratories. In recent years, significant research has been conducted to develop new nucleic acid detection methods that are more cost-effective and have simpler use and interpretation [1,2]. These methods could decentralise molecular diagnosis, thereby facilitating its implementation in resource-limited clinical settings. Furthermore, their existence would diversify the possibilities of nucleic acid sensing, avoiding the saturation of molecular diagnostics laboratories and the depletion of reagents in critical situations such as future pandemics.

Colorimetric nucleic sensors based on plasmonic materials are promising approaches for the development of cost-effective, point-of-care molecular diagnostic tools. Plasmonic nanoparticles are typically metallic nanoscale materials (1–100 nm), like gold or silver, that exhibit unique optical properties. These nanoparticles can absorb and scatter light at specific wavelengths due to their ability to support 'plasmons', collective resonance oscillations of electrons when excited by an external electromagnetic field. This effect, called Surface Plasmon Resonance (SPR), is highly dependent on the particle size, shape, and composition, being also very sensitive to the colloidal stability of the nanoparticles [3]. When these nanoparticles are in close proximity or aggregated, the effective size of the combined nanoparticle structure is increased, and the individual plasmon resonances of adjacent nanoparticles interact. This process is called plasmon coupling and causes a red shift in the plasmon spectrum [4]. Biosensors based on plasmonic gold nanoparticles (AuNPs) leverage their unique optical properties to detect and quantify biological entities. For example, the target's presence can modify the colloidal stability and aggregation state of nanoparticles that are functionalized with ligands, such as proteins or oligonucleotides, causing changes in the plasmonic signal. This shift is detected using various optical simple techniques, like colorimetry or naked-eye. In fact, these types of sensors have been used to detect proteins or RNA sequences from pathogens, including SARS-CoV-2 [5–7]. However, their sensitivity is constrained by the necessity for a sufficient quantity of the target to produce quantifiable AuNP's aggregation. Consequently, the sensitivity and selectivity of the AuNP-based sensors can be enhanced by coupling them to CRISPR/Cas target recognition [8–10]. The Class 2 CRISPR systems consist of a Cas nuclease and a guide RNA (crRNA), complementary to a target sequence, that form a ribonucleoprotein (RNP) complex. Cas13′s or Cas12′s crRNA-target interaction through base pair complementarity activates their multiple-turnover *trans*-nuclease activity. Cas12 recognizes dsDNA, while Cas13 binds ssRNA. Once activated, they cleave ssDNA (Cas12) or ssRNA (Cas13) oligonucleotides that are present in the solution. Both proteins have been successfully employed as nucleic acid biosensors [11]. Cas12 exhibits the advantage of binding and cleaving DNA, which is more stable than RNA. Nevertheless, Cas12a target recognition is limited by the necessity of a specific short sequence in the target, termed a protospacer adjacent motif (PAM). In contrast, Cas13 is not constrained by such sequence requirements, making it a more versatile option. Although the most prevalent method for determining CRISPR target recognition is through fluorescence, the utilisation of gold nanoparticles represents a promising alternative, offering the possibility of more cost-effective and straightforward approaches. Recently, we have developed a naked eye detection platform for SARS-CoV-2 called 'CASCADE' (CRISPR/CAS-based Colorimetric nucleic Acid DEtection) combining viral RNA isothermal amplification, Cas13 recognition, and AuNPs' aggregation [12]. We employed stabilised AuNPs with ssRNAs that were digested by Cas13a's *trans*-activity nuclease upon highly selective target recognition, resulting in the shortening of these AuNP-bound ssRNAs and triggering nanoparticles' aggregation (Fig. 1A).

Although the usefulness and applicability of CRISPR/AuNP-based biosensors is unarguable, there is also room for improvement regarding their read-out techniques. Naked-eye detection possesses the clear advantage of not needing equipment, but it is also prone to misinterpretation due to its subjectivity. In contrast, colorimetry readings usually rely on plate reader spectrophotometers that give more accurate information, but results can be affected by the gradual sedimentation of the reacting nanoparticles due to the self-instrument configuration. Furthermore, naked-eye and colorimetry measurements are typically read at endpoints, lacking temporal/kinetic information and ergo, the possibility of quantitative detection [6,9,13]. Time-resolved aggregation methodologies have been shown to provide more robust and quantitative information about detection reactions, being more suitable for sensing applications [14]. On the other hand, the development of user-friendly read-out techniques that do not involve the use of specialised and expensive equipment is getting more attention. In this scenario, Red-Green-Blue (RGB) colorimetric methods can be used for quantitative optical analysis of coloured solutions [15]. They are also

capable of identifying plasmonic changes, bringing more detailed information than the ordinary one-wavelength spectroscopic measurements [4]. RGB analysis has been successfully applied to correlate the AuNPs' aggregation state with the detection of different molecules, like oxytocin, formaldehyde or specific pathogens' DNA sequences, in a simple and cost-effective manner [16–18]. In these studies, digital photographs of the nanoparticles solution at reaction end-points were subjected to RGB analysis. However, the combination of real-time monitoring of AuNPs' aggregation and RGB colorimetric methods remains unexplored.

Here, we present 'CRISPR-associated Plasmonic Colorimeter Method' (Ca-PCM), an optoelectronic setup for the real-time monitoring of RNA detection by AuNP-based biosensors, using RGB colorimetric measurements. The evolution of plasmonic RGB signatures were analysed with a tailored algorithm to correlate the plasmon spectral patterns during AuNPs' aggregation with the quantitative detection of RNA. In addition, coupling Ca-PCM with previous isothermal amplification allowed the detection of RNA at fM concentration, being then suitable for RNA sensing in biological samples. In fact, we were able to detect the presence of SARS-CoV-2 RNA in real clinical samples using these implemented isothermal Ca-PCM assays. To the best of our knowledge, this is the first development of a real-time RGB analysis methodology to study AuNP-biosensors' aggregation. Moreover, this cost-effective, simple and flexible approach can be easily tuned for general nucleic acid detection from different biological sources.

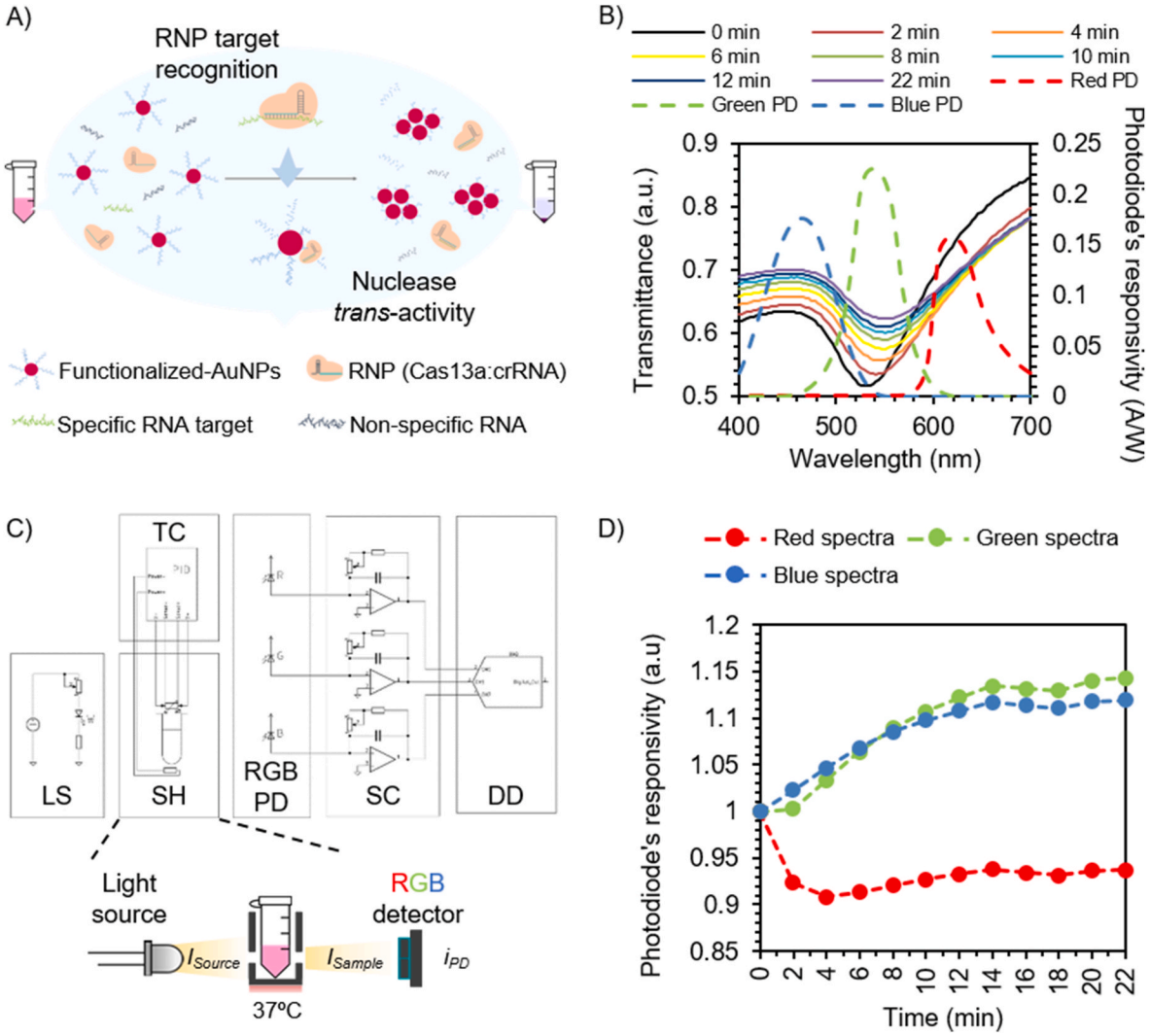

Fig. 1. CRISPR-associated Plasmonic Colorimeter Method (Ca-PCM) design and working principle. (A) Schematic representation of CRISPR/CAS-based Colorimetric nucleic Acid DEtection (CASCADE). In the absence of a specific RNA target, the ribonucleoprotein (RNP) remains inactive and ssRNA-functionalized AuNPs are stable in a saline colloidal dispersion. When the RNP recognizes the specific and complementary RNA target, its nuclease *trans*-activity is activated and cleaves ssRNAs bound to the nanoparticles. The loss of the stabilising RNA triggers AuNPs' aggregation in the saline solution promoting plasmonic changes that are visualised as a colour change of the solution. RNP: ribonucleoprotein; crRNA: guide RNA. **(B)** Transmittance spectra evolution of CASCADE sensor in the presence of a 10 nM specific target over time. UV–vis spectrum was registered every 2 min. Lines represent the mean value from three technical replicates from the same experiment (n = 3). PD's responsivity for each Red-Green-Blue channel for the indicated wavelengths is represented by a colour dashed line. A/W: ampere/watt. **(C)** Block diagram of Ca-PCM's instrumentation. LS: light source (white LED). SH: sample holder. TC: temperature control. RGB PD: RGB photodiode. SC: signal conditioning. DD: data digitization. I_{source} and I_{sample} are the light intensities before and after being transmitted through the tube, respectively. **(D)** Ca-PCM PD's temporal responsivity for the detection reaction obtained from the theoretical simulation. Data were calculated considering the intensity of the light source (I_{Source} (λ)), the intensity of the light transmitted by the sample over time (I_{Sample} (λ, t)) and the current output by the photodiode over time (i_{PD} (t)). Graph shows responsivity values over time for each Red-Green-Blue channel. (For interpretation of the references to color in this figure legend, the reader is referred to the Web version of this article.)

2. Materials and methods

2.1. Materials

Gold nanoparticles (AuNPs) of 12 nm of size (ø = 12 nm), crRNA, Cas13a, synthetic targets and oligonucleotides were synthesised or purchased as previously reported [12]. Any modification is described in the 'Supplementary Materials and Methods' section. Functionalization of AuNPs was carried out with some modifications described in the 'Supplementary Materials and Methods' section. RNA and DNA sequences are indicated in Table S1.

2.2. CASCADE reaction

CASCADE reactions were carried out as previously described with modifications [12]. Cas13a and crRNA were mixed at 1:1 molar ratio in storage buffer (20 mM Tris pH 7, 500 mM NaCl and 5 % glycerol) and incubated for 30 min at 37 °C. Then, Murine RNase Inhibitor (New England Biolabs) was added to the mixture, so the final concentration of RNP mixture was 1 μM of RNP and 4 U μL^{-1} of Murine RNase Inhibitor.

CASCADE reactions were carried out in a final volume of 100 μL. For all experiments, a master mix of functionalized-AuNPs, reaction buffer and RNP mixture was prepared and added to the samples. Each final reaction contained 5 nM of functionalized-AuNPs, RNP mixture at 5 % of the final reaction volume (50 nM of Cas13a and 50 nM of crRNA) and target RNA at the indicated concentration in reaction buffer (60 mM Tris pH 7.5, 60 mM NaCl and 6 mM $MgCl_2$). RNP mixture was added immediately before preparing the individual samples. Finally, samples were incubated at 37 °C in the indicated system.

2.3. Ca-PCM system design

An optoelectronic system to monitor colour changes in the detection reaction solution was implemented. The colorimetric subsystem consists of ten identical optoelectronic units for measuring samples in standard 1.5 mL tubes. Each optoelectronic unit consists of a white LED light source NSPW300DS (15 cd @ 20 mA and ±10°; NICHIA) that illuminates a sample contained in an aluminium cylinder to control its temperature. The light beam transmitted through the solution is detected with an RGB colour sensor S7505-01 (Hamamatsu Photonics) with a 3-channel silicon photodiode (PD) having red (R), green (G) and blue (B) sensitivities with responsivities in the bands (nm): 590–720 nm (R), 480–600 nm (G) and 400–540 nm (B). The PD photocurrents were amplified through front-end electronics based on operational amplifiers in a transimpedance configuration that adapt the signal for a digitization stage NI USB-6289 (National Instruments). This 32-channel analog-to-digital converter is controlled with LabView software, allowing the visualisation of the reaction kinetics during the experiment. In parallel, the signals generated are analysed with an in-house developed Python script, offering the quantitative analysis in real time, as detailed in the 'Supplementary Material and Methods' section.

Additionally, to ensure the proper reaction temperature at 37 °C during the whole process, each sample holder is thermally coupled to a power resistor MP915 1 % (CADDOCK) coupled at the bottom of an aluminium cylinder that thermalizes the entire reaction tube, avoiding inner condensation and thus altering the test results. Thermal control is achieved through a commercial PID (Proportional-Integral-Derivative) Model 330 Auto tuning Temperature Controller (Lake Shore Cryotronics) that monitors one channel temperature through a platinum resistor temperature sensor. This control of the experiment temperature through a single point is supported by a calibration prior to the experiment, where all the reaction tubes are characterised with dedicated thermocouples. To adjust for minor differences in each heating element and achieve 37 °C on each reaction tube, power resistors were adjusted with an individual potentiometer prior to operation. The temperature on the ten reaction tubes is monitored with a single temperature sensor in the set-up that drives the PID action.

A schematic about Ca-PCM's instrument and its working flow can be found in Fig. 1C and Fig. S2A.

2.4. Ca-PCM assay without isothermal amplification

Samples containing the indicated non-specific and specific synthetic target RNA were used in the CASCADE reaction. 20 μL of target samples were used to reach the indicated concentrations. Reactions were prepared as described above and samples were incubated inside the Ca-PCM's instrument at 37 °C until the end of the experiment. RGB transmittance intensity signals (I_R, I_G, and I_B) from each sample were recorded in real-time until the end of experiments, being visualised through LabView's software and analysed with the Python code, as described in the 'Supplementary Materials and Methods' section. In brief, the I_R, I_G, and I_B curves were used for derivatives calculation (dI/dt) to obtain the aggregation kinetics of each sample. These derivatives exhibited an 'eye-shaped pattern', formed between the B curve (top) and the R curve (bottom), being characteristic of an aggregation process, a positive identification of RNA detection. The responses for a target RNA concentration were estimated by a figure of merit we devised, a so-called 'Δ value', this being $\Delta = \max\ (dI_B/dt) - \min\ (dI_R/dt)$. The 'max' corresponds to the maximum point of the I_B derivative and 'min' to the minimum point of the I_R derivative. To find these local maxima and minima the software performs a first and second derivative test, a common mathematical method used for this kind of purpose. This method finds either the maxima or minima for a given curve by analysing its first and second derivative (since our curve is already a derivative, dI/dt, the software actually analyses the second, d^2I/dt^2, and third. d^3I/dt^3). This method is ubiquitous in calculus, it first finds proponents for local minima or maxima on a given function by identifying inflection points which are characterised by exhibiting a first derivative (second in our case) equal to zero. Inflection points however may be present in local maxima, minima and saddle points. But local maxima and minima differentiates by the concavity. Local minima exhibit a positive concavity, while local maxima exhibit a negative concavity. Concavity at the inflection points is evaluated by the positive or negative sign of its second derivative (third in our case). Therefore, these maximum and minimum values were used to calculate Δ values. Finally, a correlation between the target RNA concentration and the positive aggregation kinetics was established by plotting the log *(Δ)* versus the log *(RNA concentration)* and performing a linear regression analysis.

2.5. Three-pots/three-steps Ca-PCM assay

The amplification step consisted of two different enzymatic reactions: retrotranscription (RT)-RPA and T7 RNA transcription. RT-RPA reaction was performed by mixing an enzymatic master mix and synthetic/clinical RNA sample at a ratio of 9:1, respectively. To generate the enzymatic master mix, a previous RHB-RPA mix was prepared by resuspending 1 pellet from the TwistAmp ® Basic kit lyophilized reaction components (Twist DX) with 29.5 μL of primer free rehydration buffer (RHB) (Twist DX). Then, a primer-RT-mix was prepared that contained 1.92 μM of each primer (FW-RPA-R and RV-RPA-R; Table S1) and 7.69 U μL^{-1} of ProtoScript® II Reverse Transcriptase (New England BioLabs) in RNase-free water. The final enzymatic master mix was prepared by mixing 5.9 μL of RHB-RPA mix, 2.6 μL of primer-RT-mix and 0.5 μL of 280 mM MgAc (Twist DX). All the reaction was set up on ice. Amplification reactions containing the corresponding synthetic RNA samples were incubated at 42 °C in a conventional thermoblock during 50 min. In the case of clinical samples, the incubation time was 20 min.

T7 RNA transcription reaction was carried out in a final volume of 25 μL. Final concentration of each reagent in the transcription reaction was: 1 x Transcription Buffer (Thermo Fisher Scientific), 1 mM of each rNTP (New England BioLabs), 0.8 U μL^{-1} murine RNase inhibitor (New

England BioLabs), 0.6 U μL^{-1} T7 RNA polymerase (Thermo Fisher Scientific) and RT-RPA sample at 16 % of the final transcription reaction volume. The mixture was set up at room temperature. Reactions were incubated at 37 °C in a conventional thermoblock during 1 h. In the case of clinical samples, the incubation time was 20 min. Finally, samples were used in the Ca-PCM assay immediately or stored at −20 °C until use. Ca-PCM assay was carried out as indicated in 2.4 section using 2.5 μL from the T7 transcription reaction.

2.6. One-pot/two-steps Ca-PCM assay

One-pot RNA isothermal amplification was performed as previously described with modifications [19]. Amplification reactions consisted of an enzymatic master mix and synthetic/clinical RNA sample at a ratio of 17:3, respectively. Final concentration of each reagent in the initial enzymatic master mix was: 1.12 U μL^{-1} murine RNase inhibitor (New England BioLabs), 1.12 U μL^{-1} T7 RNA polymerase (Thermo Fisher Scientific), 2.24 U μL^{-1} Invitrogen SuperScript IV reverse transcriptase (Thermo Fisher Scientific) 0.11 U μL^{-1} RNase H (New England BioLabs), 2.24 mM of each rNTP (New England BioLabs), 0.13 μM of each primer (FW-RPA-R and RV-RPA-R; Table S1), 1 pellet from the TwistAmp Basic kit lyophilized reaction components (Twist DX), 15.65 mM magnesium acetate (Twist DX) and reaction buffer (22.4 mM HEPES pH 8, 67.1 mM KCl and 5.6 % glycerol). In the case of clinical samples, the reaction buffer was substituted by primer free rehydration buffer (Twist DX). All the components were mixed in reaction buffer, RPA pellet resuspended and then magnesium acetate added to the mixture. Mixing procedure was carried out on ice. Finally, the reaction mixture was mixed with the corresponding RNA samples and incubated at 37 °C in the Ca-PCM's instrument during 90 min. After, samples were used in the Ca-PCM assay, kept under 4 °C or stored at −20 °C for fluorescence detection ('Supplementary Materials and Methods' section). Ca-PCM assay was carried out as indicated in the 2.4 section using 10 μL of the amplified sample.

2.7. RNA extraction from clinical samples

Residual clinical nasopharyngeal samples previously tested negative or positive for SARS-CoV-2 were obtained from the Ramón y Cajal Hospital in compliance with ethical regulations and the approval of Institutional Research Ethics Committee (Code 268/24).

RNA extraction was performed on the eMAG platform (BioMérieux Spain S.A.) following the manufacturer's recommendations. Briefly, starting from 500 μL of previously anonymised nasopharyngeal samples, total RNA was eluted in 25 μL of the elution buffer. Samples were stored at −80 °C until use.

2.8. Statistical analysis

Unpaired *t*-test analysis was employed to compare each condition with the corresponding negative control. Analyses were performed using GraphPad's 'T test calculator' online tool. Threshold values for statistical significance were the following: *, $P \leq 0.05$; **, $P \leq 0.01$; ***, $P \leq 0.001$; ****, $P \leq 0.0001$.

3. Results and discussion

3.1. Development of a CRISPR-associated plasmonic colorimeter method (Ca-PCM) for monitoring AuNP-biosensors' aggregation

Our previously developed biosensor (CASCADE) [12] was based on selective target recognition by Cas13a that triggered the cleavage of ssRNA oligos exposed on the surface of functionalized-AuNPs, destabilising them and promoting their aggregation in the saline solution (Fig. 1A). This aggregative process changes the SPR over time, with a fast red-shift in the transmittance, due to initial AuNPs' aggregation. At longer times, the transmittance intensity of the plasmon spectra increases because the solution becomes more transparent due to the sedimentation of big aggregates (Fig. 1B and Fig. S1). We hypothesised that a real-time observation of these plasmonic changes employing a RGB colorimetric model would bring more detailed information about the detection process, since each spectral region would evolve differently throughout the aggregation. Therefore, it would be possible to spectrally characterise AuNPs' aggregation kinetics and correlate them with a positive detection of the RNA target. With this in mind, we designed 'CRISPR-associated Plasmonic Colorimeter Method' (Ca-PCM) as explained in the 'Materials and Methods' section. In summary, the apparatus comprises ten identical colorimeter units (Fig. 1C and Fig. S2A). The sample is maintained in standard 1.5 mL tubes within an aluminium cylinder, which is thermally coupled to a power resistor heater, allowing for the control of its temperature. A white LED light source is used to illuminate each sample, and the transmitted light is detected by an RGB sensor. This RGB sensor consists of a 3-channel silicon photodiode (PD) which is used to detect red (R) (from 590 to 720 nm), green (G) (from 480 to 600 nm) and blue (B) (from 400 to 540 nm) light. The RGB signals are then amplified by a transimpedance amplifier and digitised by an analogue-to-digital converter in order to be visualised by LabView software and finally analysed on a Python script. Thus, this system consisted of a simple measurement device made by commercial and highly available components (Table S3), being then suitable for clinical environments with low resources.

Real-time measurement was assured using this configuration, because the light beam was transmitted transversally to the direction of the sedimentation of the nano-aggregates, so the optical signal is not affected by the gradual sedimentation during the reaction, in contrast with microplate reader instruments where the light beam illuminates the sample vertically. Furthermore, our approach allowed the direct analysis of the RGB intensities, allowing the visualisation of their real-time evolution, in contrast to previous works focused on measuring total absorbance or using digital photographs where RGB values were mathematically retrieved [16,18,20]. In parallel to the design and implementation of the instrument, we validated the method with a theoretical simulation of the plasmonic spectra variation during AuNPs' aggregation. This approximation tried to replicate temporal evolution of the RGB signals as if captured by the instrument. For this purpose, we used the transmittance spectral values from a CASCADE reaction measured at different time points in a conventional plate reader spectrophotometer (Fig. 1B) and transformed them to the RGB temporal signals following the analysis presented in the 'Supplementary Results and Discussion' section (Figs. S2B and S2C). We obtained the time evolution of the three transmittance intensity signals: I_R, I_G, and I_B. As presented in Fig. 1D, the aggregation of AuNPs would produce plasmon-coupling effects with a red-shift in the plasmon resonance, decreasing the red transmittance. This generates a reduction of the I_R, and an increase of the I_B. The I_G also is increased, delayed from the blue signal. This simulation suggested that each I_R, I_G, and I_B curves would evolve in a different way during the aggregation. Therefore, the three temporal parameters could be used to capture and characterise the plasmonic changes associated to the detection reaction.

Finally, we tested the developed Ca-PCM for the real detection of a synthetic RNA sequence (R target) that resembles a SARS-CoV-2 genetic region that is recognised by Cas13a's crRNA (Table S1). A non-specific sequence from SARS-CoV-2 (NS-target), not complementary to the crRNA, was used as negative control (Table S1). The system recorded RGB intensities in real-time and results were represented. Experimental read-outs (Fig. 2) agreed with the theoretical simulation (Fig. 1D). A rapid decrease in the red signal was observed, produced by the red-shift of the plasmon signal through aggregation. The blue signal change is delayed over the red signal, because it is mainly influenced by the sedimentation process and the increase of transmittance intensity that it produced (Fig. 1B and Fig. S1). The temporal evolution of the I_G intensity was more complex, with a fast decrease during the first minutes,

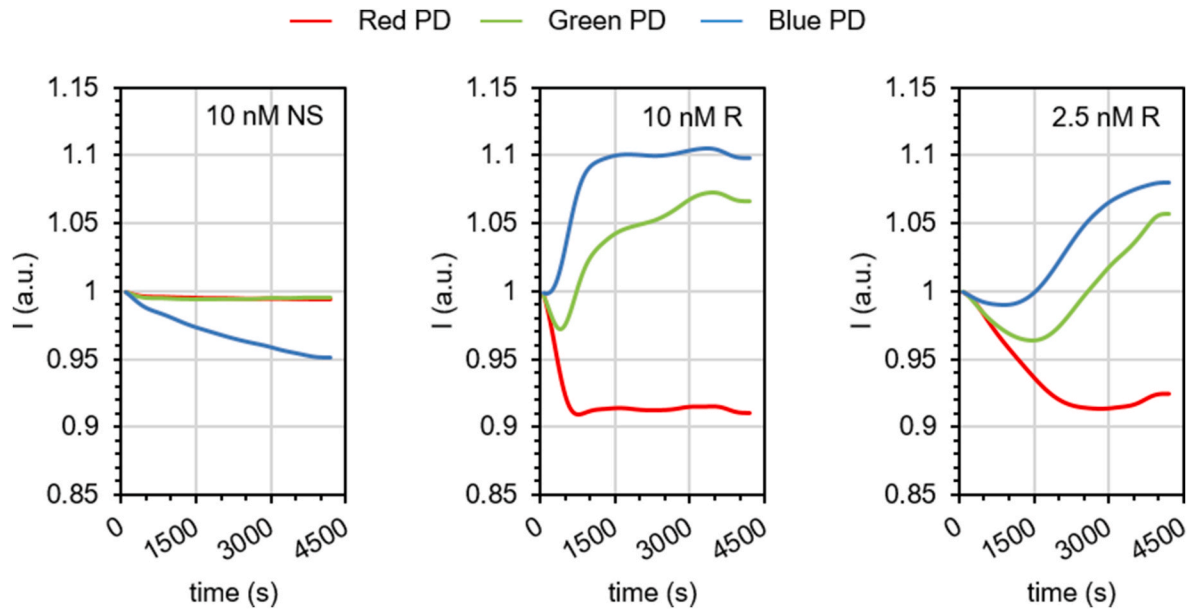

Fig. 2. Real-time RGB intensity curves obtained from the Ca-PCM. 10 nM of non-specific (NS) target and 10 and 2.5 nM of specific (R) target were subjected to Ca-PCM. Graphs show RGB intensity signals (*I*, being I_R, I_G and I_B) evolution during one representative experiment. a.u.: arbitrary units.

similar to I_R, due to the red-shift of the plasmon spectra. Later, the higher transparency of the solution produced the I_G increment. This RGB evolution was produced by the presence of the target, since the intensities for the non-specific control (left graph in Fig. 2) were stable for every experiment tested (n = 5). The results clearly showed that Ca-PCM was capable of capturing the plasmonic coupling changes that occur during AuNPs' aggregation as a consequence of target detection. It relied on the real-time behaviour of three spectrally integrated intensities (I_R, I_G and I_B) measured simultaneously, being then a robust method. The results were plotted with Labview during the experiments, allowing the monitorization of the reaction in a user-friendly manner. Finally, in contrast with other approaches that use RGB analysis from images or time point captures [16,18], to the best of our knowledge, this is the first time the RGB model is applied in real-time, providing continuous, non-treated and direct measurements. This new methodology could constitute a relevant improvement for the monitoring of biosensors based on plasmonic nanoparticles.

Interestingly, the slope of each RGB signal temporal change, that described the aggregation speed, seemed dependent on the specific target concentration (Fig. S3). A higher target concentration led to higher slopes, suggesting the potential of this methodology as a quantitative tool. Target RNA interaction with Cas13a triggers its *trans*-nuclease activation, meaning that target concentration was directly related to enzyme concentration. An increase in target concentration, and therefore in active Cas13a concentration, accelerated the cleavage of ssRNA bound to AuNPs and therefore, promoted a faster AuNP's aggregation.

3.2. Ca-PCM combined with isothermal amplification

Ca-PCM was capable of sensing RNA at nM-pM levels (Fig. S3), in line with previously described sensitivity of CRISPR detection techniques without prior sample amplification [21]. However, most nucleic acid targets are present at lower concentration in biological samples [22,23]. We and other groups have demonstrated that sensitivity of CRISPR-Cas-based methods can be increased by adding a previous isothermal amplification reaction [12,24,25]. RPA (Recombinase Polymerase Amplification) is one of the most used nucleic acid amplification techniques for CRISPR-based sensors because of its simplicity of design and execution, fast speed and sensitivity. We coupled our previously established RT-RPA reaction [12] to Ca-PCM. It consisted of three-pots/three-steps reactions (RT-RPA, T7 transcription and CASCADE) that promote CRISPR target recognition and subsequent AuNPs' aggregation. Fig. 3A and Fig. S4 showed that Ca-PCM detected the amplified RNA, resembling the aggregation kinetics observed previously for non-amplified samples (Fig. 2).

However, this RNA amplification method required subsequent reaction steps that could increase the risk of sample contamination and false positive results. To overcome this problem, one-pot RNA sensing reactions have already been successfully developed [19]. We tested a modified version of this one-pot amplification method using our SARS-CoV-2 target and a fluorescence read-out method [24], showing that it amplified the RNA target in a dose-dependent manner [19] (Fig. S5). Once coupled with Ca-PCM read-out, a one-pot/two-step reaction was developed: an initial one-pot enzymatic RNA amplification, and a final detection reaction. In brief, one-pot RNA amplifications were carried out inside the device at 37 °C during 90 min and then, a mixture of Cas13a RNP and functionalized AuNPs was added to the amplified samples. The RGB kinetics obtained using the one-pot/two steps Ca-PCM (Fig. 3B and Fig. S6) resembled the results obtained from amplification-free experiments (Fig. 2 and Fig. S3), although a delayed starting point and lower RGB amplitudes were obtained in comparison to amplification-free samples (Figs. 2 and 3B). These differences could be explained by low RNA concentration present after amplification and/or changes in the media due to the presence of reagents needed for amplification reaction. We also observed that functionalized AuNPs' stability was slightly compromised in some non-specific controls. It has been described that biological molecules such nucleic acids and proteins can interact with the surface of AuNPs affecting their colloidal stability [26]. Thus, some components from the RPA reaction mix could be affecting nanoparticles' stability. However, this unspecific effect was delayed in comparison to the one produced by Cas13a's positive detection (Fig. 3B and Fig. S6).

It is worth mentioning that the same RGB evolution pattern over time is observed for the direct detection of synthetic RNA and for both types of pre-amplification reactions, showing Ca-PCM read-out's robustness and flexibility to be adapted to different amplification reactions.

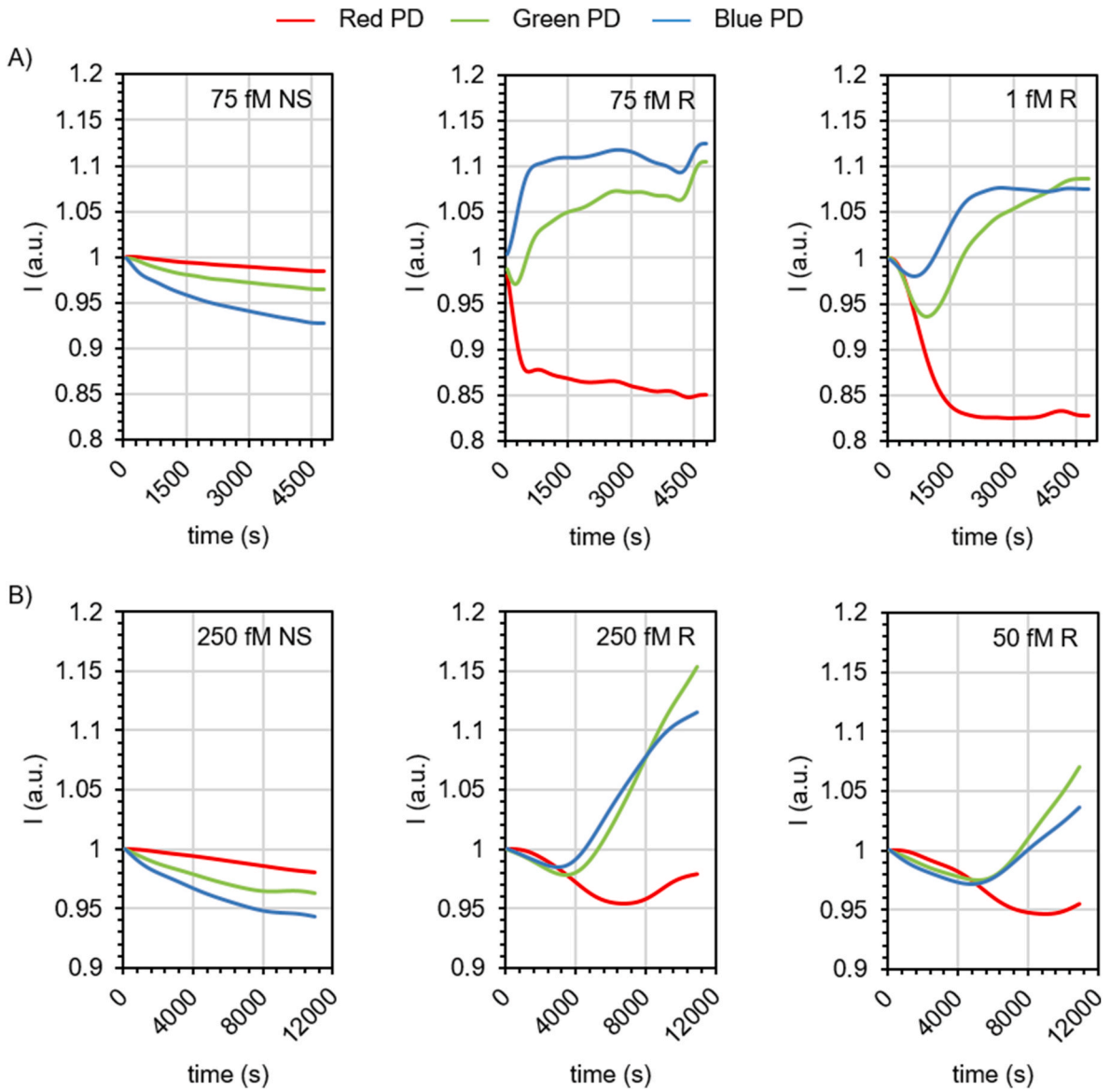

Fig. 3. Real-time RGB intensity curves obtained from the isothermal Ca-PCM assays. (A) 75 fM of non-specific (NS) target and 75 and 1 fM of specific (R) target were subjected to three-pot/three-steps Ca-PCM assay. **(B)** 250 fM of non-specific (NS) target and 250 and 50 fM of specific (R) target were subjected to one-pot/two-steps Ca-PCM. Intensity transmittance signals were recorded and data conditioned employing the automatic code. Graphs show RGB intensity signals (I) over time of a representative experiment. a.u.: arbitrary units.

3.3. Algorithm development for automatic-quantitative RNA detection by Ca-PCM

The consistent RGB kinetic experimental profiles obtained by the three types of samples tested (Figs. 2 and 3) with specific targets defined a 'fingerprint' of the reactions, a potential unequivocal way to detect a positive detection. However, it could be difficult to directly observe these changes at very low target concentration. With this in mind, we developed a mathematical algorithmic analysis of the RGB kinetics to clearly define the pattern of detection and also to quantify the parametric changes produced by target concentration. As mentioned before, the rate of change in the intensity signals was dependent on the RNA concentration. Derivatives of each spectral temporal trace (dI/dt) were then obtained and plotted (Fig. 4 and Figures S7, S8 and S9). Results showed that RGB derivatives formed an evident 'eye-shaped pattern' between the derivative I_B curve (upper) and I_R curve (lower). This was consistent with the RGB intensity evolution of raw data seen in Figures S3, S4 and S6. This particular shape was common to all aggregation events that contained specific RNA (Figure S7–9), for all the performed assays, independently on the existence and type of pre-amplification steps, a sort of characteristic 'fingerprint'.

Once we identified the aggregation pattern, we developed different analytical methods and Python algorithms to strictly and automatically identify positive samples and obtain quantitative data ('Supplementary Results and Discussion' section and Figs. S10 and S11). The results of one-pot/two-steps Ca-PCM were used at this step, as they mimicked the most convenient conditions to be used in clinical settings. The chosen identification algorithm (Table S4) relied on two conditions that must be accomplished: a local minimum with a positive concavity in the red derivative curve, followed by a local maximum with a negative concavity in the blue one (Fig. 4). The first and second derivative test method was used to find these local max and min (Fig. S11). A complete description of the method can be followed in the 'Materials and Methods' and 'Supplementary Materials and Methods' sections. Samples that did not satisfy the aforementioned conditions were automatically classified as negative by the algorithm. However, some negative samples

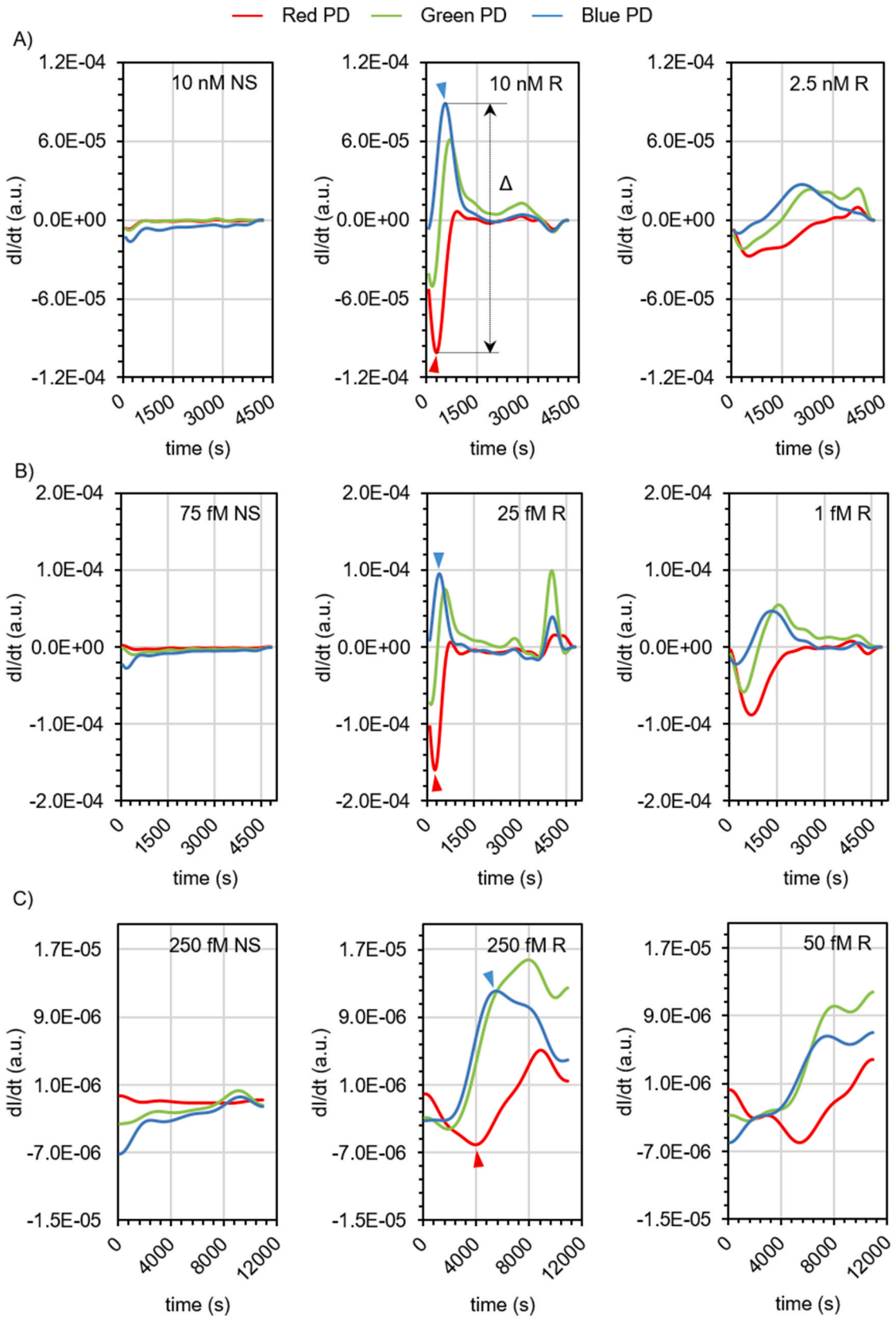

Fig. 4. Derivatives of real-time RGB signals. Non-specific RNA target (NS) and different concentrations of specific target (R) were tested by Ca-PCM, three-pots/three-steps Ca-PCM assay or one-pot/two-steps Ca-PCM. **(A)** Derivative signals of each Ca-PCM spectral trace over time for the indicated target concentrations. Blue arrow points out the maximum point of the blue derivative. Red arrow points out the minimum point of the red derivative. Δ indicates the difference between the maximum point of the blue derivative and the minimum point of the red derivative. **(B)** Derivative signals of each three-pots/three-steps Ca-PCM spectral trace over time for the indicated target concentrations. **(C)** Derivative signals of each one-pot/two-steps Ca-PCM spectral trace over time for the indicated target concentrations. (For interpretation of the references to color in this figure legend, the reader is referred to the Web version of this article.)

exhibited local minimum and maximum values due to random signal noise. Figure S7–9 showed that the difference between red minima and blue maxima (i.e. maximum slope or speed), increased with higher RNA concentrations, being very small in negative control samples. This property was used to define a new variable, 'delta' (Δ = max (dI_B/dt) – min (dI_R/dt)), that described aggregation speed (Fig. S10). Both max (dI_B/dt) and min (dI_R/dt) were already calculated by the first and second derivative test. When applied to results from the detection without previous amplification, we could clearly identify positive detections using the Δ value of the non-specific sample as a threshold (Fig. 5A). Accordingly, the system presented a two-level mechanism for the detection of positive samples. Firstly, the presence of an eye-pattern in the derivative RGB intensities must be established by the algorithm. Secondly, a Δ value higher than that obtained in a non-specific sample is required. This implies that a control non-specific sample must be analysed concurrently with the tested samples, or that a threshold Δ value must be calculated with precision. This is a common method used to discriminate between positive and negative samples in detection methods, such as qPCR [27,28], or Sherlock [29].

Fig. 5A showed that Δ values were dependent on RNA target concentration (active Cas13a's concentration). They did not follow a linear correlation (Fig. S12), due to Cas13a's mechanism to induce AuNP's aggregation: many AuNP-bound ssRNAs should be cleaved to expose enough AuNPs' surface to trigger their aggregation. In addition, other processes like steric hindrances between enzymes to interact with those ssRNAs when the active Cas13a concentration increases cannot be ruled out. A linear correlation was obtained using a double logarithmic representation (Fig. 5B) ($R^2 = 0.975$). This correlation highlights the potential of Ca-PCM as a quantitative approach for AuNP-based RNA detection, being a clear advantage from previous biosensing methods that use AuNPs' aggregation as a read-out and lack kinetic and quantitative information [12,13]. In addition, the automatic implementation of Δ calculation and linear regression analysis in the same algorithm suppose an easy and timesaving manipulation for the final user.

Moreover, to study the repeatability of the technique, we conducted repeated experiments using 5 nM and 2.5 nM of R specific target, and 5 nM of non-specific target (Table S5). The coefficient of variation (CV (%)) for all samples is lower or equal to 10 %, below the recommended value to consider a reliable biosensor [30].

In order to ensure the reliability and versatility of the designed algorithm, our Ca-PCM was employed to detect different sequences. To this end, the specificity of RNP was modified by employing distinct RNA guides (crRNA) to target alternative sequences, including ZIKV and a region of the SARS-CoV-2 S gene. Following the recognition of the specific RNA by the RNP, AuNPs' aggregation occurred, and was captured by the RGB photodiodes, resulting in the formation of eye-shaped patterns (Fig. S13) that allowed the automatic measurement of the corresponding Δ values (Fig. S14). The Δ value of positive samples was found to be higher than that obtained with the non-specific control, with the exception of ZIKV at 25 nM, being then considered negative. Additionally, the Δ value was dependent on the sample concentration for both types of sequences. These findings validated the robustness of the algorithm across different RNA sequences. They were also a proof of the specificity of our system. Overall, three different sequences were used as non-specific controls: NS region in Fig. 5, SARS-CoV-2 R region in Figs. S14A–B and ZIKV region in Figs. S14C–D. All these controls resulted in very small Δ values, lower than the specific samples.

The Δ analysis of three-pots/three-steps amplified samples (Fig. 5C) showed that the algorithm detected the presence of the target. The non-specific target and the lower concentration of target did not present the eye pattern fingerprint in their derivatives (Fig. S8) and no Δ values were calculated (Fig. 5C). Target concentrations higher or equal to 1 fM showed a clear eye-pattern (Fig. S8), with Δ values higher than the ones obtained with non-amplified synthetic RNA. However, Δ is not dependent on target concentration (Fig. 5D). Ca-PCM recognition is dose-dependent, therefore the pre-amplification reaction is not quantitative. Indeed, previous research had demonstrated that typical RPA reaction is not a quantitative amplification methodology. Rather, it has been developed to generate the maximum number of amplicons [24].

When the algorithm was applied to results from one-pot/two-steps Ca-PSM, Δ analysis (Fig. 5E) revealed that non-specific Δ values were lower than the ones from the specific target concentrations (n = 5). Interestingly, the obtained Δ values were dose-dependent, and a linear correlation between the logarithmic values of Δ and starting RNA concentration was obtained ($R^2 = 0.954$) (Fig. 5F). It suggested that one-pot amplification is slower than three-pots, so once Cas13a and AuNPs were added for read-out (after 90 min), the amplification was already at the exponential phase. Thus, dose-dependency is achieved, although Δ values obtained (Fig. 5E) are lower than in the three-pots configuration (Fig. 5C). This dose dependency can be also observed using fluorescence as a read-out (Fig. S5), supporting this hypothesis. To further investigate the system's robustness and dose-dependency, we compared the results obtained by one-pot/two-steps Ca-PCM and two gold-standard methods: RT-qPCR and CRISPR recognition coupled with fluorescence read-out (Fig. S15). Results from several experiments showed a positive linear correlation between our one-pot/two steps Ca-PCM and the two methodologies (Fig. S15), highlighting Ca-PCM's potential as a biosensing technique, comparable to standard methods.

For both amplification methods, Ca-PCM was able to detect RNA at a concentration as low as 1 fM, as it is statistically significant over the negative control (Fig. 5C and E). Furthermore, the LoD of our one-pot/two-steps sensor, calculated using an already published empirical method [31], is 2.26 fM (see Supplementary Information and Table S6), being thus sensitive enough for RNA detection in biological sources. These target concentrations correspond to 10^3 viral SARS-CoV-2 copies μL^{-1}, a similar detection limit to commercial LFD SARS-CoV-2 viral antigen immunoassays that can detect medium viral loads (Ct < 25) [32].

3.4. Detection of RNA in clinical samples by Ca-PCM

Finally, we tested the suitability of Ca-PCM for RNA sensing in clinical samples from patients that were previously diagnosed as negative or positive for SARS-CoV-2 infection by RT-qPCR. Three independent measurements per sample were performed to assure the reliability of the technique. The three-pot/three-steps Ca-PCM system clearly discriminated between negative and positive samples, using as threshold the Δ value of the non-specific (NS) sample. In fact, it detected SARS-CoV-2 in all the samples with Ct below 28 (Fig. 6A and Fig. S16).

The one-pot/two-steps configuration yielded comparable outcomes (Fig. 6B and Fig. S17), but showing lower Δ values, which can be attributed to the levels of amplification reached by the isothermal technique. The negative samples were all correctly identified as such in the three experiments conducted using our method. Samples with a cycle threshold (Ct) value below 28 were identified as positive in all three experiments, with the exception of P2 in Experiment 1, which is likely attributable to a random error. Moreover, P13, with a cycle threshold (Ct) value of 30, was identified by our method in three out of the three experiments. Overall, 36 of the 39 positive samples were identified as positive by Ca-PCM, indicating a positive predictive value (PPV) of 92 % (PPV 97 % for samples with Ct below 28) (Table 1). It is also noteworthy that the negative predictive value (NPV) is 100 %, ruling out the possibility of false positive results. Moreover, the Δ values exhibited an inverse correlation with the Ct values, as anticipated. However, this was only observed in samples with a Ct value above 18. Samples with a higher viral load exhibited a lower Δ than anticipated. The same behaviour was observed for the three-pots/three-steps Ca-PCM. It can therefore be inferred that this phenomenon is independent of the amplification method and can be attributed to the gold nanoparticles. Indeed, Ca-PCM experiments using synthetic RNA without amplification at high RNA concentrations presented Δ values lower than expected (Fig. S18), suggesting that an excess of RNA in the solution

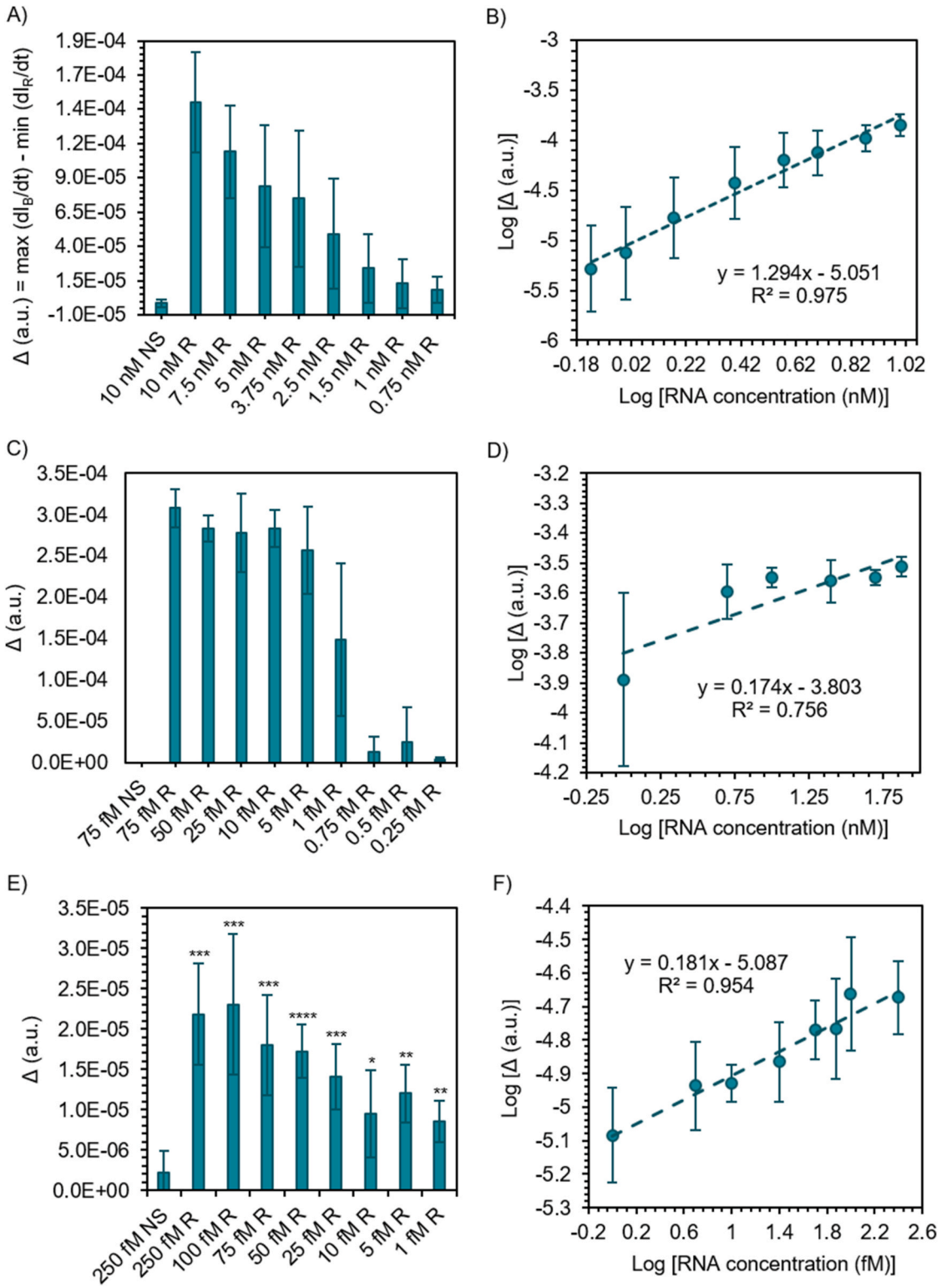

Fig. 5. RNA detection by Ca-PCM and isothermal Ca-PCM assays. Non-specific (NS) target and the indicated concentrations of specific (R) target were employed in Ca-PCM **(A–B)**, three-pots/three-steps Ca-PCM assay **(C–D)** or one-pot/two-steps Ca-PCM assay **(E–F)**. Intensity signals for each photodiode were recorded and their derivatives analysed by the automatic algorithm. **(A)** Δ values obtained for the different target concentrations. Bars represent the mean value of five independent experiments (n = 5) ± SD. **(B)** Correlation between reaction speed (*log [Δ]*) and specific target concentration (*log [RNA concentration (nM)]*) from 10 to 0.75 nM conditions. Dots represent the mean value from five independent experiments (n = 5) ± SD. **(C)** Δ values obtained for the different target starting concentrations. Bars represent the mean value of three independent experiments (n = 3) ± SD. **(D)** Correlation between reaction speed (*log [Δ]*) and specific target concentration (*log [RNA concentration (nM)]*) from 75 to 1 fM conditions. Dots represent the mean value from three independent experiments (n = 3) ± SD. **(E)** Δ values obtained for the different target concentrations. Bars represent the mean value of five independent experiments (n = 5) ± SD. **(F)** Correlation between (*log [Δ]*) and specific target concentration (*log [RNA concentration (nM)]*) from 250 to 1 fM conditions. Dots represent the mean value from five independent experiments (n = 5) ± SD. SD: standard deviation. R^2: linear regression coefficient. a.u.: arbitrary units. *: $P \leq 0.05$; **: $P \leq 0.01$; ***: $P \leq 0.001$; ****: $P \leq 0.0001$.

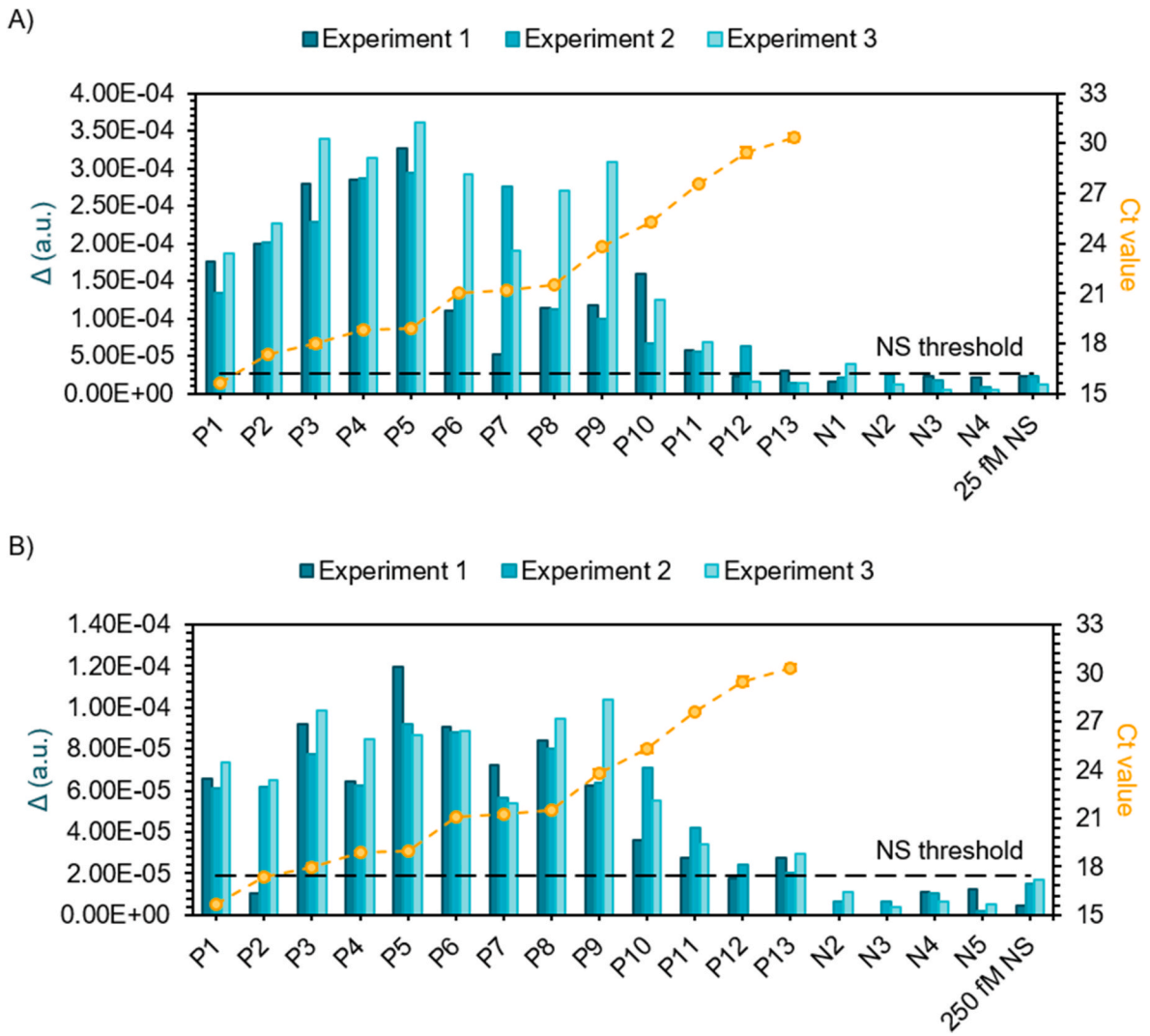

Fig. 6. Three-pots/three-steps and one-pot/two-steps Ca-PCM assays' applicability in clinical samples. Clinical samples tested as negative (N1-5) or positive (P1-13) for the presence of SARS-CoV-2 by RT-qPCR were employed in the three-pots/three-steps Ca-PCM assay **(A)** or one-pot/two-steps Ca-PCM assay **(B)**. Dots represent the mean Ct value from one experiment (n = 1) performed in triplicates ± SD. Non-specific target (NS) at the indicated starting concentration was used as a negative control for positive sample discrimination. **(A)** Δ values obtained from the three-pots/three-steps Ca-PCM assay and their corresponding Ct values obtained from RT-qPCR for each clinical patient. Samples were evaluated by Ca-PCM assay in three independent experiments. Black dashed line represents the NS threshold calculated by the sum of its Δ mean value and its corresponding SD from the three independent experiments. **(B)** Δ values obtained from the one-pot/two-steps Ca-PCM assay and their corresponding Ct values obtained from RT-qPCR for each clinical patient. Samples were evaluated by Ca-PCM assay in three independent experiments. Black dashed line represents the NS threshold calculated by the sum of its Δ mean value and its corresponding SD from the three independent experiments. SD: standard deviation.

Table 1
Concordance between one-pot/two-steps Ca-PCM and RT-qPCR assays for 51 patients' Ca-PCM determinations. RT-qPCR assay was performed once in triplicates. Table shows the number of negative (−) and positive (+) results obtained by each assay.

		One-pot/two-steps Ca-PCM assay	
		−	+
RT-qPCR assay	−	12	0
	+	3	36

could stabilise the gold nanoparticles and slow down the aggregation. In conclusion, the one-pot/two-step Ca-PCM approach is a dose-dependent methodology, even when employed with clinical samples, in contrast to conventional AuNP-based techniques. However, the correlation is constrained to medium viral loads (Ct between 18 and 28), a limitation that must be taken into account when using the method in clinical settings. In conclusion, these results demonstrated the robustness of our system for its potential application in real diagnosis, presenting enough sensitivity to diagnose infective patients at similar levels to SARS-CoV-2 antigen tests. The method is both cost-effective and straightforward, and therefore readily applicable in clinical settings. All reagents and kits are commercially available, as well as the PCM components. Furthermore, the PCM configuration and the algorithm are sufficiently simple to be easily reproduced by individuals with a basic understanding of optics. However, the implementation of this technique requires the involvement of trained personnel in sample collection and RNA extraction, which may restrict its broader clinical application. Nevertheless, it could prove to be a valuable option in hospital facilities of low-income countries.

Finally, Ca-PCM offers a high degree of adaptability, as numerous parameters can be adjusted to suit different purposes. For example, alternative isothermal amplification techniques could be employed [12], and the method could be readily adapted to detect additional

pathogens by modifying the Cas13's crRNA. Despite that, it should be carefully considered that the sensitivity of CRISPR-based sensors is dependent on the specific crRNA and RNA target design employed. This is evidenced by the differing recognition observed for the R region of the SARS-CoV-2 virus (Fig. 5A) in comparison to the S region or ZIKV RNA (Fig. S14). Consequently, it is essential to design the optimal crRNA for each target detection, a process that can be time-consuming.

4. Conclusions

Our results clearly demonstrated that the proposed Ca-PCM constitutes a robust technique for nucleic acid detection based on AuNPs' aggregation. It requires inexpensive instrumentation (Table S3) in comparison with typical nucleic-acids detection techniques like qPCR or fluorescence coupled CRISPR methods. The necessary components for the assembly of the equipment are readily available on the commercial market and represent a cost-effective solution. Furthermore, the configuration is straightforward and can be readily reproduced. In contrast with other biosensors that use endpoint measurements to discriminate between positive or negative readings, the real-time RGB model can be successfully applied to characterise the plasmonic changes that occur during the detection reaction, correlating it with detection of the target in a dose dependent manner thanks of the obtention of kinetic information. This working principle could be also useful for other biosensing methods that rely on the aggregation of plasmonic nanoparticles in a colloidal solution because of biological target recognitions, such as antibodies, viral particles or antigens. Moreover, Ca-PCM assay coupled with pre-amplification methods was sensitive enough to detect RNA for biological applications, like the detection of pathogens in clinical samples, showing a PPV of 97 % for SARS-CoV-2 clinical samples with Ct $<$ 28. Finally, yet importantly, it works with trivial data read-out in a user-friendly manner, constituting a potential candidate as a method for molecular diagnosis in low-resource clinical environments that cannot afford costly and specialised techniques. In conclusion, Ca-PCM represents a promising new nucleic acid detection method with the potential to expand the portfolio of molecular diagnosis techniques even further.

CRediT authorship contribution statement

Hernán Alarcón-Iniesta: Writing – original draft, Visualization, Methodology, Investigation. **Guillermo de Arana:** Writing – original draft, Visualization, Software, Methodology. **María López-Valls:** Resources, Methodology, Investigation. **Demian Pardo:** Resources. **Carmen Escalona-Noguero:** Methodology, Investigation. **Ciro Rodríguez:** Methodology, Investigation. **Milagros Castellanos:** Methodology, Conceptualization. **Sara Cobelo:** Methodology. **Isidoro Martínez-Ramírez:** Software. **Julio Camarero:** Project administration, Conceptualization. **Sergio de las Heras:** Resources. **Javier de Vicente:** Resources. **Andrés Valera:** Resources. **Warren Smith:** Resources. **Ramón Bernardo-Gavito:** Conceptualization. **Rafael Cantón:** Resources. **Juan Carlos Galán:** Resources, Methodology, Investigation. **Daniel Granados:** Conceptualization. **Rodolfo Miranda:** Supervision, Funding acquisition. **Héctor Guerrero:** Writing – review & editing, Writing – original draft, Visualization, Supervision, Project administration, Conceptualization. **Begoña Sot:** Writing – review & editing, Writing – original draft, Visualization, Supervision, Project administration, Conceptualization.

Declaration of competing interest

The authors declare that they have no known competing financial interests or personal relationships that could have appeared to influence the work reported in this paper.

Acknowledgements

This work was supported by the Spanish Ministry of Economy and Competitiveness (PID2020-119352RB-I00), Spanish Ministry of Science, Innovation and Universities (PID2023-146982OB-I00) and Madrid Regional Government (NANOCOV-CM). RBG thanks "Ayuda de Atracción de Talento de la Comunidad de Madrid (2019-T2/IND-13367)". IMDEA Nanociencia acknowledges support from the 'Severo Ochoa' Programme for Centres of Excellence in R&D (Spanish Ministry of Economy and Competitiveness, Grant SEV-2016-0686, CEX2020-001039-S).

We would like to thank Alvaro Somoza (IMDEA Nanociencia) for useful data discussion and Irene Pardo (IMDEA Nanociencia) for her help handling the RNA from clinical samples.

Appendix B. Supplementary data

Supplementary data to this article can be found online at https://doi.org/10.1016/j.aca.2024.343601.

Data availability

Data will be made available on request.

References

[1] T. Ming, et al., Advancements in biosensors for point-of-care testing of nucleic acid, Crit. Rev. Anal. Chem. (2024) 1–16.
[2] Y.P. Zhang, et al., Advances in rapid point-of-care virus testing, Analyst 149 (9) (2024) 2507–2525.
[3] M. Soler, L.M. Lechuga, Principles, technologies, and applications of plasmonic biosensors, J. Appl. Phys. 129 (11) (2021) 111102.
[4] J.L. Montano-Priede, et al., Robust rules for optimal colorimetric sensing based on gold nanoparticle aggregation, ACS Sens. 8 (4) (2023) 1827–1834.
[5] P. Moitra, et al., Selective naked-eye detection of SARS-CoV-2 mediated by N gene targeted antisense oligonucleotide capped plasmonic nanoparticles, ACS Nano 14 (6) (2020) 7617–7627.
[6] C. Rodriguez Diaz, et al., Development of colorimetric sensors based on gold nanoparticles for SARS-CoV-2 RdRp, E and S genes detection, Talanta 243 (2022) 123393.
[7] B.D. Ventura, et al., Colorimetric test for fast detection of SARS-CoV-2 in nasal and throat swabs, ACS Sens. 5 (10) (2020) 3043–3048.
[8] Y. Cao, et al., CRISPR/Cas12a-mediated gold nanoparticle aggregation for colorimetric detection of SARS-CoV-2, Chem. Commun. 57 (56) (2021) 6871–6874.
[9] L. Ma, et al., CRISPR-Cas12a-Powered dual-mode biosensor for ultrasensitive and cross-validating detection of pathogenic bacteria, ACS Sens. 6 (8) (2021) 2920–2927.
[10] Z. Zhao, et al., Nanomaterials-assisted CRISPR/Cas detection for food safety: advances, challenges and future prospects, TrAC, Trends Anal. Chem. 167 (2023).
[11] C. Escalona-Noguero, M. Lopez-Valls, B. Sot, CRISPR/Cas technology as a promising weapon to combat viral infections, Bioessays 43 (4) (2021) e2000315.
[12] M. Lopez-Valls, et al., CASCADE: naked eye-detection of SARS-CoV-2 using Cas13a and gold nanoparticles, Anal. Chim. Acta 1205 (2022) 339749.
[13] W.S. Zhang, et al., Reverse transcription recombinase polymerase amplification coupled with CRISPR-cas12a for facile and highly sensitive colorimetric SARS-CoV-2 detection, Anal. Chem. 93 (8) (2021) 4126–4133.
[14] P. Barik, J. Banerjee, M. Pradhan, Real-time probing of melamine-induced gold nanoparticle aggregation kinetics via evanescent-wave coupled cavity ring-down spectroscopy, Anal. Chem. 95 (24) (2023) 9357–9365.
[15] G. de Carvalho Oliveira, et al., RGB color sensor for colorimetric determinations: evaluation and quantitative analysis of colored liquid samples, Talanta 241 (2022) 123244.
[16] W. Huang, et al., RGB color analysis of formaldehyde in vegetables based on DNA functionalized gold nanoparticles and triplex DNA, Anal. Methods 14 (36) (2022) 3598–3604.
[17] L. Ma, et al., A smartphone-based visual biosensor for CRISPR-Cas powered SARS-CoV-2 diagnostics, Biosens. Bioelectron. 195 (2022) 113646.
[18] S. Rastogi, et al., RGB colorimetric method based detection of oxytocin in food samples using cysteamine functionalized gold nanoparticles, Anal. Biochem. 656 (2022) 114886.
[19] J. Arizti-Sanz, et al., Streamlined inactivation, amplification, and Cas13-based detection of SARS-CoV-2, Nat. Commun. 11 (1) (2020) 5921.
[20] I. Reinhard, et al., Nanoparticle design rules for colorimetric plasmonic sensors, ACS Appl. Nano Mater. 3 (5) (2020) 4342–4350.
[21] H. Shinoda, et al., Amplification-free RNA detection with CRISPR-Cas13, Commun. Biol. 4 (1) (2021) 476.

[22] R. Arnaout, et al., The limit of detection matters: the case for benchmarking severe acute respiratory syndrome coronavirus 2 testing, Clin. Infect. Dis. 73 (9) (2021) e3042–e3046.
[23] R. Emmadi, et al., Molecular methods and platforms for infectious diseases testing a review of FDA-approved and cleared assays, J. Mol. Diagn. 13 (6) (2011) 583–604.
[24] J.S. Gootenberg, et al., Nucleic acid detection with CRISPR-Cas13a/C2c2, Science 356 (6336) (2017) 438–442.
[25] A. Kostyusheva, et al., CRISPR-Cas systems for diagnosing infectious diseases, Methods 203 (2022) 431–446.
[26] J.W. Lee, S.R. Choi, J.H. Heo, Simultaneous stabilization and functionalization of gold nanoparticles via biomolecule conjugation: progress and perspectives, ACS Appl. Mater. Interfaces 13 (36) (2021) 42311–42328.
[27] D. Dutta, et al., COVID-19 diagnosis: a comprehensive review of the RT-qPCR method for detection of SARS-CoV-2, Diagnostics 12 (6) (2022).
[28] K. Linkowska, et al., Commercially available SARS-CoV-2 RT-qPCR diagnostic tests need obligatory internal validation, Sci. Rep. 13 (1) (2023) 6991.
[29] M. Patchsung, et al., Clinical validation of a Cas13-based assay for the detection of SARS-CoV-2 RNA, Nat. Biomed. Eng. 4 (12) (2020) 1140–1149.
[30] L.C. Chen, et al., Improving the reproducibility, accuracy, and stability of an electrochemical biosensor platform for point-of-care use, Biosens. Bioelectron. 155 (2020) 112111.
[31] D.A. Armbruster, T. Pry, Limit of blank, limit of detection and limit of quantitation, Clin. Biochem. Rev. 29 (Suppl 1) (2008) S49–S52. Suppl 1.
[32] T. Peto, COVID-19: rapid antigen detection for SARS-CoV-2 by lateral flow assay: a national systematic evaluation of sensitivity and specificity for mass-testing, EClinicalMedicine 36 (2021) 100924.